

ECAFormer: Low-light Image Enhancement using Cross Attention

Yudi Ruan¹, Hao Ma², Weikai Li^{1*}, Xiao Wang^{2*}

¹School of Mathematics and Statistics, Chongqing Jiaotong University, Chongqing, 400074, China

²School of Artificial Intelligence, Anhui University, Hefei, AnHui, 230039, China

Abstract

Low-light image enhancement (LLIE) is critical in computer vision. Existing LLIE methods often fail to discover the underlying relationships between different sub-components, causing the loss of complementary information between multiple modules and network layers, ultimately resulting in the loss of image details. To beat this shortage, we design a hierarchical mutual Enhancement via a Cross Attention transformer (ECAFormer), which introduces an architecture that enables concurrent propagation and interaction of multiple features. The model preserves detailed information by introducing a Dual Multi-head self-attention (DMSA), which leverages visual and semantic features across different scales, allowing them to guide and complement each other. Besides, a Cross-Scale DMSA block is introduced to capture the residual connection, integrating cross-layer information to further enhance image detail. Experimental results show that ECAFormer reaches competitive performance across multiple benchmarks, yielding nearly a 3% improvement in PSNR over the suboptimal method, demonstrating the effectiveness of information interaction in LLIE.

Introduction

Capturing images in low-light conditions presents significant challenges in computer vision, including the degradation of fine details, reduced color saturation, diminished contrast and dynamic range, and uneven exposure. These issues can greatly compromise the integrity and clarity of captured data, negatively impacting the effectiveness of subsequent applications such as autonomous driving systems (Ranft and Stiller 2016; Cai et al. 2020; Bresson et al. 2017) and nighttime surveillance efforts (Fu et al. 2021). Naturally, enhancing the visibility of objects and details in low-light images is crucial, possessing far-reaching implications for a spectrum of vision applications.

Currently, efforts for LLIE have predominantly utilized deep-learning techniques, which can be categorized into three main approaches: Conventional, Guided, and Two-Branch Methods, as depicted in Figure 1. Conventional methods, such as LLNet (Lore, Akintayo, and Sarkar 2017) and UFormer (Wang et al. 2022), hinge on data-driven strategies and tailored loss functions but are constrained by

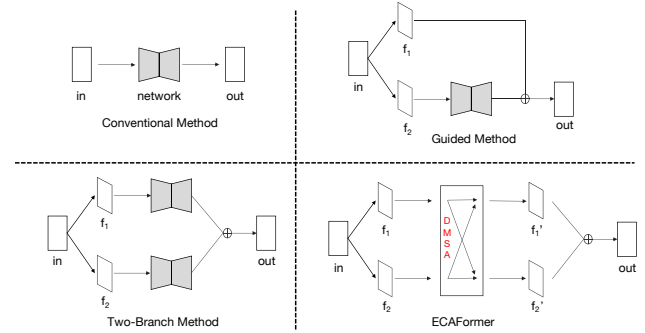


Figure 1: Main architecture comparison. Compared to other methods, our approach utilizes DMSA to simultaneously propagate two features forward and facilitate interactions at different scales. This method is advantageous for extracting latent connections between features.

data complexity, hindering the model’s ability to capture robust representations. To overcome this, guided methods integrate prior knowledge into LLIE. They decompose the input into essential and target components, leveraging the former knowledge to guide the enhancement of the latter through specialized networks. For example, some guided methods based on Retinex theory (Land and McCann 1971) focus on preserving the consistency of the reflection component while adjusting the illumination. Another line to integrate prior knowledge is the Two-Branch Methods (Ma et al. 2021; Tang et al. 2022), which further refine the input by separating it into distinct sub-components, each processed by dedicated enhancement networks. However, despite the use of prior knowledge, these methods may overlook the interrelationships among components in the latent space. This limitation, inherent in the model architecture, can result in a loss of image details during enhancement.

Regarding the current situation in the LLIE field, we focus on enhancing the information interactions across different components and layers to fill in the image details. Specifically, we proposed a Hierarchical Mutual Enhancement via a Cross Attention transformer (ECAFormer) as shown in Figure 2. To achieve this, we employ the U-shaped architecture as the foundation of our model to enhance low-light

*Corresponding Authors

images. Following the idea of two branch methods, we incorporate a knowledge-driven strategy that decomposes images into distinct visual and semantic components, which facilitates detail preserving with the guidance of semantic information. Further, to fully leverage the advantages of both, we integrate a modified transformer to harness visual and semantic components. In order to enhance the interactions across different sub-components in the latent space, we designed Dual Multi-head Self-Attention (DMSA) to handle multiple inputs, capturing potential relationships between different components. Notably, the transition from Multi-Head Self-Attention (MHSA) in the vanilla transformer to DMSA modules is strategically designed to simultaneously exploit both long- and short-range dependencies within the image data. Moreover, to further preserve the details, we also design a Cross-Scale DMSA to foster an interplay between residual and current layer information, which is ingeniously leveraged to refine the residual connections within ECAFormer. Our main contribution can be summarized as follows:

- We explore a novel LLIE method named **ECAFormer**, which illustrates the importance of information integration across layers and components for detail preservation in LLIE.
- We collect a novel *Traffic-297* dataset, which includes various traffic scenes and provides a new benchmark in LLIE.
- We achieve competitive results on six LLIE datasets emphasizing computational frugality and parameter parsimony.

Related Work

LLIE: Low-light Image Enhancement

Currently, the rapid advancement in low-light image dataset collection has led to the emergence of numerous deep learning-based enhancement methods (Li et al. 2021). LLNET (Lore, Akitayo, and Sarkar 2017) introduced a variant of the stacked sparse denoising autoencoder for improving degraded images, establishing a foundational framework for the application of deep learning in image enhancement. RetinexNet (Wei et al. 2018) employed a deep Retinex-based architecture to enhance low-light images by decomposing them into illumination and reflectance components. RUAS (Liu et al. 2021) utilized an advanced search unfolding technique based on a Retinex architecture. EnlightenGAN (Jiang et al. 2021) innovatively used a generative inverse network as the primary framework, initially training with unpaired images. LEDNet (Zhou, Li, and Loy 2022), is a robust network specifically designed to address the dual challenges of low-light enhancement and deblurring simultaneously.

However, these methods primarily rely on Convolutional Neural Networks (CNN) models as their backbone and do not fully leverage global information or feature interaction for LLIE, resulting in detail loss. This paper proposes a transformer model with cross attention module that utilizes the global perception ability of transformers to deeply fuse visual and semantic features.

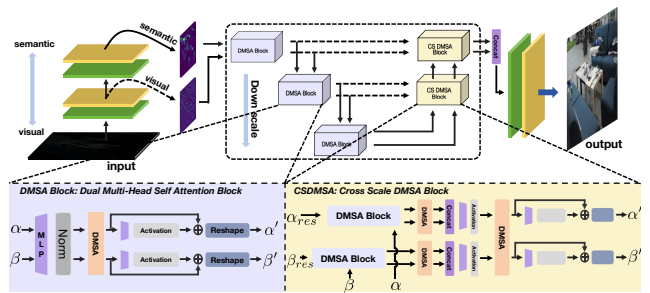


Figure 2: The flowchart of ECAFormer

Components Decomposition and Fusion

Compared to conventional LLIE methods, the components decomposition and fusion techniques have more effectively captured the latent knowledge within the data and significantly enhanced model performance. Among these approaches, feature combination frameworks can be classified into two types, as illustrated in Figure 1: (1) Two-Branch Methods, which optimize distinct features using separate networks, such as CSDGAN (Ma et al. 2021) and DRLIE (Tang et al. 2022); (2) Guided Methods, which use one feature to guide the optimization of another feature, exemplified by SNRNet (Xu et al. 2022).

However, the aforementioned model architectures fail to fully leverage the complementary information between the decomposed sub-components, often treating them too independently and hindering the network from learning the intrinsic relationships between multiple sub-components. Therefore, we propose the DMSA module, which can simultaneously handle and inter-relate two features during forward computation. This modification enables the model to learn the relationships between sub-components, integrating their respective advantages and mitigating biases from ideal assumptions, thus improving the final output of the model.

Methodology

In this section, we present a comprehensive description of each network module proposed and the corresponding loss functions employed. Inspired by the successful U-shaped architecture in LLIE (Li et al. 2021), we introduce a transformer network with a U-shaped architecture, depicted in Figure 2. Specifically, ECAFormer comprises three main components: (1) Visual-semantic convolution module, which generates short-range features (visual-features) and long-range features (semantic-features). (2) The U-shaped cross attention Transformer interacts with long- and short-term input features through DMSA, simultaneously propagating these features. (3) Mapping convolution, where the module projects the interacted features back to image features $\in \mathbb{R}^{C \times H \times W}$. In practice, the low-light input image undergoes convolution filtering to extract semantic information and visual detail information respectively. The enhanced image is then obtained through interaction enhancement of a U-shaped network using semantic and visual features.

Problem Definition

Low-light image enhancement aims to mitigate the challenges associated with low brightness, low contrast, noise, and artifacts in images captured under inadequate lighting conditions. These issues arise from the loss of visual information due to insufficient illumination or complex environmental factors at the time of image capture. The objective of low-light image enhancement is to utilize models to restore and enhance low-light images \mathbb{L} , bringing them closer to normal images \mathbb{N} and rendering them more perceptible to the human visual system.

The problem can be mathematically modeled as follows:

$$\hat{I} = f(I, \theta), \quad (1)$$

where $I \in \mathbb{R}^{C \times H \times W}$ represents the input low-light images \mathbb{L} , $\hat{I} \in \mathbb{R}^{C \times H \times W}$ represents the enhanced images, and θ represents the parameters of the network function f .

The objective of the optimization process is to find the optimal parameters θ that minimize the differences between the enhanced images and the reference high-light or normal images \mathbb{N} . This can be formulated as:

$$\hat{\theta} = \arg \min_{\theta} \ell(\hat{I}, R), \quad (2)$$

where $R \in \mathbb{R}^{C \times H \times W}$ denotes the well-exposed reference or normal images, and ℓ denotes the loss function used to guide the network.

Model Framework

Preliminary In LLIE, CNNs are adept at extracting intricate local features, while Transformer networks excel in capturing valuable global feature information from complex environments. As the depth of the convolution layers increases in CNNs, the extracted features progressively embody richer semantic information. Consequently, features obtained from initial shallow convolution operations are predominantly visual, while those derived from deeper convolution layers contain more sophisticated semantic insights. To capitalize on these characteristics, we have developed a decoupling convolution extractor, which decouples the image to the visual and semantic features.

$$\begin{aligned} f_v &= \text{Conv}_1(I), \\ f_s &= \text{Conv}_2(f_v), \end{aligned} \quad (3)$$

where f_v retains an abundance of detailed visual features, while f_s preserves advanced semantic features. Both attributes are pivotal for achieving the enhanced final result.

The attention mechanism facilitates interactivity among elements, significantly enhancing global feature extraction capabilities. The conventional self-attention mechanism is defined by Eq. 4, where the vectors Q , K , and V represent query, key, and value derived from a single input. This operation selectively focuses on crucial information, optimizing resource utilization and swiftly capturing the most relevant data. Leveraging this advantage, we have developed a unique Dual Multi-head Self-Attention module (DMSA) to facilitate the fusion of two distinct features. This module processes two inputs and enables their interaction via the

attention mechanism while preserving their dimensional integrity. A detailed discussion of this module will be provided later.

$$\text{MHSA}(Q, K, V) = \text{softmax} \left(\frac{QK^T}{\sqrt{d_k}} \right) V. \quad (4)$$

We have developed a U-shaped network structure with enhanced residual information, specifically tailored to improve the network’s capacity for multi-scale interaction. This architecture facilitates a comprehensive synthesis of features across various scales. During the down-sampling phase, we strategically employed a $2 \times$ scaling factor to compel the network to undergo a rigorous compression process, as we separate the image into visual and semantic features. This intentional compression is crucial as it allows the network to extract more refined global information, which is essential for understanding broader contextual cues. The methodology and details of the down-sampling stage are illustrated in Eq. 5.

$$[f_v, f_s]^{(i)} = \text{RS}(\text{DMSA}_i([f_v, f_s]^{(i-1)})), \quad (5)$$

where $\{i \in 1, 2\}$ denotes the step of the down-sample stage, $\text{RS}(\cdot)$ represents the resample operation, the DMSA_i denotes the DMSA Block varies at i stages. At the bottom of the U-shaped network, we used a bottleneck consisting of two DMSA modules. And in the up-sampling process, we employed operations proportional to down-sampling. During the up-sampling phase, we utilized CSDMSA to effectively retain and restore intricate details that are often lost during the down-sampling process through residual information. The residual information initially engages in cross attention with their corresponding features, followed by cross attention between the two types of features in the CSDMSA block. This process is crucial in maintaining the fidelity of feature representations, ensuring that the reconstructed outputs closely resemble the original inputs. Finally, we obtain the final output through concatenation and mapping convolution. It can be represented by Eq. 6.

$$\hat{I} = \mathcal{A}_{agg} \left(f_v^{(T)}, f_s^{(T)} \right). \quad (6)$$

Visual-Semantic Convolution Module Inspired by the potent capability of convolution layers to enhance local features, we devised a visual-semantic convolution module specifically designed to capture local characteristics. In CNNs, as the number of convolution layers increases, the receptive field of the model progressively enlarges, leading to the extraction of increasingly complex semantic features as shown in Figure 3. It can be observed that visual feature f_v focuses more on fine details, while semantic feature f_s emphasizes broader connections and contextual relationships within the image. However, this expansion often results in the attenuation of fine-grained detail within the features. To address this, we introduce a dedicated convolution module that outputs two distinct types of features: f_v and f_s . Here, f_v is derived from shallow convolution layers, capturing detailed visual features, whereas f_s emanates from deeper convolution layers, encapsulating higher-level semantic information. Additionally, the CNNs can capture periodic and local spatial features, addressing the spatial context induction

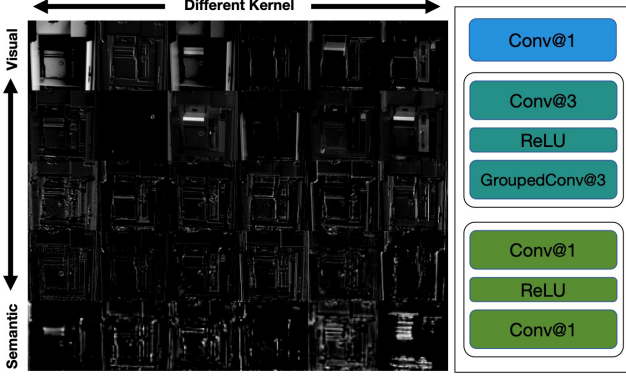


Figure 3: From top to bottom are the shallow outputs and deep outputs of the model, respectively.

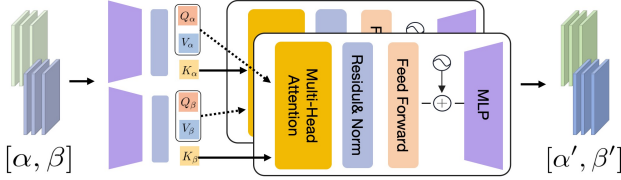


Figure 4: Architecture of DMSA

bias in transformers that rely solely on positional embedding. We employ depth-wise separable convolution within this module to enhance the rate of forward propagation without compromising much accuracy. Upon processing through this module, the network then employs attention mechanisms to facilitate a dynamic interaction between these two distinct features.

DMSA Self-attention is highly efficient at directing concentrated attention toward pivotal information, thereby optimizing resource utilization and rapidly acquiring the most relevant data. However, its standard configuration is restricted to processing only a single input, which can limit its applicability in scenarios requiring complex interactions between multiple data streams. To address this constraint, we have innovated the Dual Multi-head Self Attention (DMSA) module as shown in Figure 4, a sophisticated mechanism designed to effectively manage and integrate dual inputs. In this module, inputs α and β are processed to generate distinct sets of Q , K , and V vectors through separate mappings. We strategically cross the key vectors of both inputs within this module to enhance their inter-connectivity, fostering a richer, more comprehensive interaction. This is achieved by the multiplication of the query vector with the corresponding crossed key vector, producing an attention map that encapsulates the intricate dynamics between the two inputs. Enhanced by the adaptive sampling operations of the U-shaped network, this setup facilitates a profound interaction across multiple scales, allowing for a nuanced integration of features that is essential for complex analysis and interpretation

tasks.

$$\text{DMSA}(Q_\alpha, K_\beta, V_\alpha) = \text{softmax}(Q_\alpha K_\beta^T * \zeta) V_\alpha. \quad (7)$$

The scaling factor ζ is determined through optimization. To preserve the spatial positional relationships among pixels, we have incorporated a position embedding ($PosEmb$) module, executed via convolution operations. Consequently, the output of the Dual Multi-head Self Attention module $[\alpha', \beta']$ can be formally defined in Eq. 8.

$$[\alpha', \beta'] = [\text{DMSA}(Q_\alpha, K_\beta, V_\alpha) + \text{PosEmb}(V_\alpha), \text{DMSA}(Q_\beta, K_\alpha, V_\beta) + \text{PosEmb}(V_\beta)]. \quad (8)$$

CSDMSA During the downsampling process, detail loss often leads to image blurring, making the utilization of residual information crucial. To address this, we employ a specially designed Cross-Scale Dual Multi-head Self Attention (CSDMSA) module to handle cross-layer residual information, aiming to reduce image degradation.

First, the residual and intermediate features are processed by the DMSA module as follows:

$$\begin{aligned} [\alpha'_{res}, \alpha'_{mid}] &= \text{DMSA}([\alpha_{res}, \alpha_{mid}]), \\ [\beta'_{res}, \beta'_{mid}] &= \text{DMSA}([\beta_{res}, \beta_{mid}]), \end{aligned} \quad (9)$$

where α_{mid} and β_{mid} represent the features of the current layer, while α_{res} and β_{res} correspond to the residual information, respectively. Next, we concatenate the corresponding features to facilitate subsequent interaction operations:

$$\begin{aligned} \alpha_{agg} &= W \cdot \text{concat}([\alpha'_{res}, \alpha'_{mid}]) + B, \\ \beta_{agg} &= W \cdot \text{concat}([\beta'_{res}, \beta'_{mid}]) + B, \end{aligned} \quad (10)$$

where α_{agg} and β_{agg} represent the features after fusion, W is the learned weight matrix and B is the learned bias matrix. Finally, the interaction between α_{agg} and β_{agg} is processed through another DMSA module, followed by a resampling operation. The final output $[\alpha', \beta']$ of the CSDMSA module is given by:

$$\begin{aligned} [\alpha', \beta'] &= \text{CSDMSA}([\alpha, \beta]) \\ &= \text{RS}(\text{DMSA}([\alpha_{agg}, \beta_{agg}])), \end{aligned} \quad (11)$$

where $\text{RS}(\cdot)$ denotes the resampling operation.

Loss Function

We incorporated two types of loss functions that better align with human visual perception and facilitate faster model training. The Total Loss \mathcal{L}_{Total} can be represented as Eq. 12, $\lambda \in [0, 1]$.

$$\mathcal{L}_{Total} = \lambda * \mathcal{L}_p + (1 - \lambda) * \mathcal{L}_c, \quad (12)$$

where \mathcal{L}_p is the loss of perceptual and \mathcal{L}_c is the loss of charbonnier.

Perceptual Loss Perceptual Loss (Johnson, Alahi, and Fei-Fei 2016) adopts an efficient approach by quantifying the discrepancies through the squared error between features extracted from specific layers or an aggregation of multiple

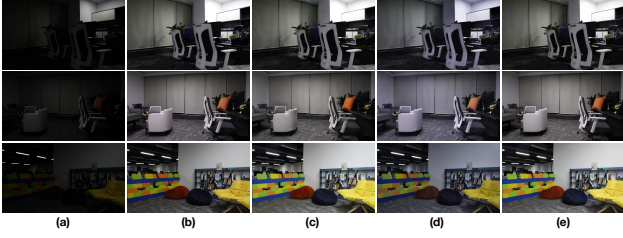


Figure 5: Three images from SDSD-indoor test set were selected for comparison with different methods. (a) Input Image. (b) Ground Truth. (c) ZeroDCE++. (d) SNRNet. (e) ECAFormer.

layers after both the ground truth and the reconstructed image have traversed the same pre-trained neural network. The Perceptual Loss \mathcal{L}_p is given as follows:

$$\mathcal{L}_p = \sum_{i=1}^n \frac{1}{C_i H_i W_i} |F_i^l(f(I)) - F_i^l(R)|^2. \quad (13)$$

Among them, f symbolizes the enhancement network. F_i^l indicates the i -th feature map in the l -th layer. We have utilized a VGG-19 network pre-trained on ImageNet and employed the output feature maps from its initial five ReLU layers to compute the loss. This method leverages the deep network’s architecture to extract rich, complex feature representations that are critical for assessing the perceptual quality of the enhanced images.

Charbonnier Loss Compared to the conventional L_1 Loss, Charbonnier Loss exhibits superior robustness and stability, particularly when dealing with outliers. Additionally, the computational efficiency of Charbonnier Loss is enhanced due to its reliance on a single square and root operation, in contrast to the ordinary L_1 Loss which necessitates an absolute value computation. This streamlined calculation speeds up the processing and contributes to smoother gradients, facilitating more effective optimization during model training. The Charbonnier Loss \mathcal{L}_c is given as follows:

$$\mathcal{L}_c = \sum_{i=1}^n \sqrt{(\hat{I} - R)^2 + \epsilon^2}. \quad (14)$$

Benefiting from the addition of epsilon, the phenomenon of gradient vanishing when \hat{I} and R are very close has been alleviated, making the model easier to train.

Experiment

Experimental Configurations

Datasets We conducted comparisons across multiple public datasets: LOL-v1 (Wei et al. 2018), LOL-v2 (Yang et al. 2021b), SID (Chen et al. 2019), SMID (Chen et al. 2018), and SDSD (Wang et al. 2021). Additionally, we have collected the *Traffic-297* dataset, which includes various traffic scenes. It contains an amount of real nighttime traffic scenes with complex lighting environments, which pose a significant challenge to low-light enhancement models.

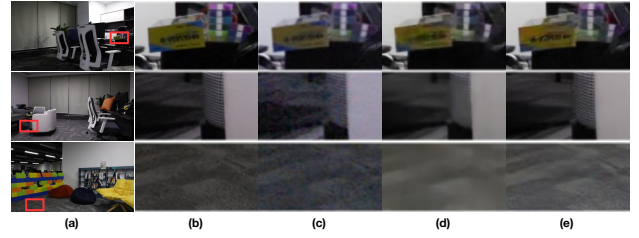


Figure 6: The detailed comparison of the three images selected from SDSD-indoor test set. (a) Indicator. (b) Ground Truth. (c) ZeroDCE++. (d) SNRNet. (e) ECAFormer.

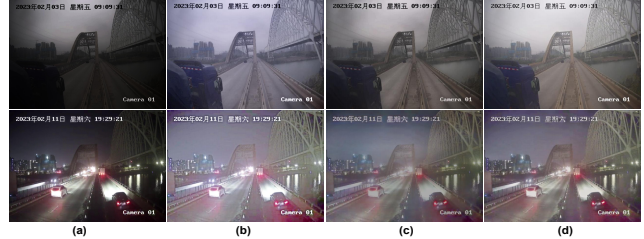


Figure 7: Visual detail comparison on the Traffic-297. (a) Input Image. (b) ZeroDCE++. (c) SNRNet. (d) ECAFormer.

Implementation Details We implemented the ECAFormer model using PyTorch. The model was trained on an NVIDIA RTX 4090 with 24 GB of VRAM using the Adam optimizer ($\beta_1 = 0.9$ and $\beta_2 = 0.999$), across a total of 250,000 iterations. The initial learning rate was set at 2×10^{-4} and gradually reduced to 1×10^{-6} through a cosine annealing schedule during the training process. Training samples were generated by randomly cropping 128×128 patches from pairs of low-/normal-light images. The batch size was set to 8. The training data was augmented with random rotations and flips to enhance variability and robustness. The training objective was to minimize both \mathcal{L}_p and \mathcal{L}_c between the enhanced images and their corresponding ground truths, ensuring high fidelity in the restoration of image details and color accuracy. To evaluate the performance, we employ the peak signal-to-noise ratio (PSNR) and structural similarity index (SSIM) (Wang et al. 2004) as the primary metrics for evaluation.

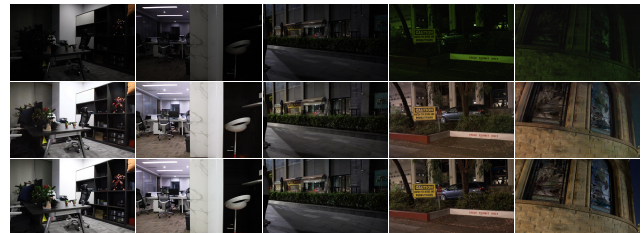


Figure 8: The experimental results across different scenes. From the first row to the third row are (1) Input Image. (2) ECAFormer. (3) Ground Truth.

	UF	RN	EnGAN	RUAS	DRBN	KinD	RSTM	LLF	MIRNet	SNR	ECAFormer
LOL-v1	16.36	16.77	17.48	18.23	20.13	20.86	22.43	23.65	24.14	24.61	<u>24.24</u>
LOL-v2-r	18.82	15.47	18.23	18.37	20.29	14.74	19.94	20.06	20.02	<u>21.48</u>	21.99
LOL-v2-s	19.66	17.13	16.57	16.55	23.22	13.29	21.41	24.04	21.94	<u>24.14</u>	25.86
SID	18.54	16.48	17.23	18.44	19.02	18.02	22.27	-	20.84	<u>22.87</u>	24.69
SMID	27.20	22.83	22.62	25.88	26.6	22.18	26.97	-	25.66	<u>28.49</u>	29.34
SDSD-in	23.17	20.84	20.02	23.17	24.08	21.95	25.67	-	24.38	29.44	<u>29.11</u>
SDSD-out	23.85	20.96	20.10	23.84	25.77	21.97	24.79	-	27.13	<u>28.66</u>	29.57
Average	21.08	18.64	18.89	20.64	22.73	19.00	23.35	-	23.44	<u>25.67</u>	26.40
FLOPS(G)	12.00	587.47	61.01	0.83	48.61	34.99	144.25	22.52	785.00	26.35	27.34
Params(M)	5.29	0.84	114.35	0.003	5.27	8.02	26.13	24.55	31.76	4.01	2.50

Table 1: Comparison of PSNR across 7 public datasets using different methods. ECAFormer achieved promising results with the least number of parameters.

Comparison Methods To validate the effectiveness of our derived ECAFormer, we conducted extensive comparisons with several state-of-the-art conventional, two branch and guided LLIE approaches. For the conventional LLIE, we compared the UFormer(UF) (Wang et al. 2022), EnlightenGAN(EnGAN) (Jiang et al. 2021), Restormer(RSTM) (Zamir et al. 2022), LLFormer(LLF) (Wang et al. 2023), and MIRNet (Zamir et al. 2020). For the two-branch LLIE, we compared the RUAS (Liu et al. 2021), DRBN (Yang et al. 2021a) and KinD (Zhang, Zhang, and Guo 2019). For the guided LLIE, we compared the RetinexNet(RN) (Wei et al. 2018) and SNR-Net (Xu et al. 2022).

Results Analysis

Quantitative Results To validate the quantitative performance of ECAFormer, we compared our model across seven public datasets using two metrics, PSNR and SSIM, with the results presented respectively in Table 1 and Table 2. The results on our collected *Traffic-297* dataset are shown in Table 3. Specifically, our ECAFormer achieves a 3% improvement in PSNR and nearly a 1% improvement in SSIM over the suboptimal method. As we can observe, our ECAFormer demonstrates a 3% improvement in PSNR and nearly a 1% improvement in SSIM over the suboptimal method. The results indicate that our model achieves competitive performance while maintaining a relatively low parameter count and computational complexity.

Quality Results To validate the quality performance of ECAFormer, we present the visual comparison of the results, as shown in Figure 5-7. As we can observe, the recent fully supervised learning method, SNRNet, did not retain sufficient detail and exhibited blurring. ZeroDCE++, which adjusts the pixel curves, introduced excessive noise. In the detailed comparison illustrated in Figure 6, our method effectively preserves texture details while considering global brightness balance, indicating its ability to retain details and suppress noise. In Figure 8, we showcase the performance of our model across different scenes, including color discrepancies caused by nighttime shooting. Specifically, our method was tested in complex scenarios from

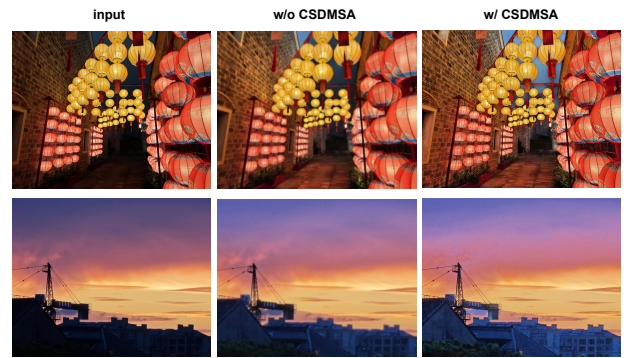


Figure 9: The ablation experiment of CSDMSA. Without the CSDMSA module, the images become blurred.

SDSD-in, SDSD-out, and SMID datasets, with results indicating strong performance of ECAFormer. In Figure 7, we evaluated the performance in traffic scenes, specifically testing models trained on synthesized datasets under real-world nighttime scenarios. The complexity of lighting conditions in nighttime traffic scenes poses a significant challenge to models. While other methods may introduce noise and lose details, our model demonstrates exceptional visual performance by effectively preserving details while considering global illumination. In comparison, ZeroDCE++ exhibits overexposure issues, highlighting the superior visual results of our proposed model. These results indicate that our model adapts well to variations and produces high-quality outcomes closely approximating the ground truth, demonstrating the effectiveness of ECAFormer as proposed in this paper.

Ablation Study

To assess the efficacy of the different modules, including 1) Visual-Semantic Feature (VSF), 2) Loss, and 3) DMSA, we made adjustments to the model structure and presented the PSNR results in given Table 4 and Figures 9 - 10. The results presented in Table 4 suggest that all three components positively impact the model’s performance and are effective.

	UF	RN	EnGAN	RUAS	DRBN	KinD	RSTM	LLF	MIRNet	SNR	ECAFormer
LOL-v1	0.771	0.560	0.650	0.720	0.830	0.790	0.823	0.816	0.830	<u>0.842</u>	0.850
LOL-v2-r	0.771	0.567	0.617	0.723	0.831	0.641	0.827	0.792	0.82	<u>0.849</u>	0.853
LOL-v2-s	0.871	0.798	0.734	0.652	0.927	0.578	0.830	0.909	0.876	<u>0.928</u>	0.931
SID	0.577	0.578	0.543	0.581	0.577	0.583	<u>0.649</u>	-	0.605	<u>0.625</u>	0.660
SMID	0.792	0.684	0.674	0.744	0.781	0.634	<u>0.758</u>	-	0.762	<u>0.805</u>	0.810
SDSD-in	0.859	0.617	0.604	0.696	0.868	0.672	0.827	-	0.864	0.894	<u>0.874</u>
SDSD-out	0.748	0.629	0.616	0.743	0.841	0.654	0.802	-	0.837	0.866	<u>0.862</u>
Average	0.769	0.633	0.634	0.694	0.807	0.650	0.788	-	0.799	<u>0.829</u>	0.834

Table 2: Comparison of SSIM across 7 public datasets using different methods

	RN	ZeroDCE++	EnGAN	SNR	ECAFormer
PSNR	18.56	18.35	18.19	<u>30.06</u>	33.26
SSIM	0.770	0.884	0.623	<u>0.965</u>	0.978

Table 3: Comparison of PSNR and SSIM on the traffic-297 dataset

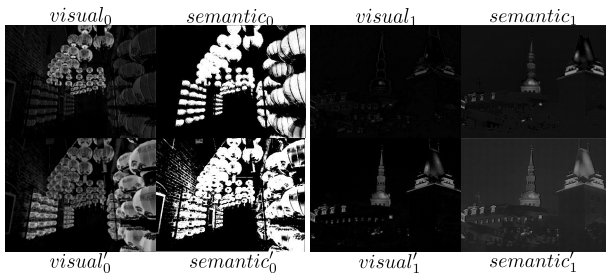


Figure 10: Visualization of the two features before and after interaction through DMSA. The first row shows before interaction, and the second row shows after interaction.

Among them, the DMSA module shows the most significant improvement in feature fusion.

Furthermore, in ECAFormer, we utilize the DMSA module to effectively manage cross-layer residual information, thereby minimizing the loss of details resulting from downsampling. This validates the capability of CSDMSA module to integrate residual information, as depicted in Figure 9. It is evident that without the CSDMSA module, the enhanced images suffer from blurring and significant loss of image detail. This outcome indicates that the CSDMSA module effectively mitigates the loss of details caused by downsampling by utilizing cross-layer residual information.

Besides, as depicted in Figure 10, DMSA effectively facilitates the seamless integration of visual and semantic features. The findings demonstrate that visual features complement semantic features by providing additional intricate details, while semantic features offer long-range dependencies for visual features, resulting in improved brightness uniformity. Therefore, our designed DSMA significantly enhances the complementary information of visual and semantic features.

VSF	Loss	DMSA	PSNR(avg)
	✓	✓	28.56
✓		✓	29.41
✓	✓		28.38
✓	✓	✓	29.57

Table 4: Ablation study results on SDSD-out

Conclusion

In this paper, we propose a transformer-based method for LLIE, specifically utilizing DMSA blocks to enhance low-light images. Furthermore, the ECAFormer network combines the advantages of local detailed feature information extraction in CNNs and global information extraction in transformer networks. Therefore, ECAFormer is capable of extracting both global and local information from the image. Extensive experimental results validate the competitive advantages of ECAFormer compared to other state-of-the-art algorithms. In our future research, we will focus on refining the training approach to enable the model to effectively utilize disparate datasets and integrate additional prior knowledge to enhance its feature extraction capabilities. This is particularly important as ECAFormer currently relies on paired images, which significantly complicates the process of dataset collection.

References

- Bresson, G.; Alsayed, Z.; Yu, L.; and Glaser, S. 2017. Simultaneous localization and mapping: A survey of current trends in autonomous driving. *IEEE Transactions on Intelligent Vehicles*, 2(3): 194–220.
- Cai, P.; Sun, Y.; Wang, H.; and Liu, M. 2020. VTGNet: A vision-based trajectory generation network for autonomous vehicles in urban environments. *IEEE Transactions on Intelligent Vehicles*, 6(3): 419–429.
- Chen, C.; Chen, Q.; Do, M. N.; and Koltun, V. 2019. Seeing motion in the dark. In *Proceedings of the IEEE/CVF International conference on computer vision*, 3185–3194.
- Chen, C.; Chen, Q.; Xu, J.; and Koltun, V. 2018. Learning to see in the dark. In *Proceedings of the IEEE conference on computer vision and pattern recognition*, 3291–3300.

- Fu, L.; Yu, H.; Juefei-Xu, F.; Li, J.; Guo, Q.; and Wang, S. 2021. Let there be light: Improved traffic surveillance via detail preserving night-to-day transfer. *IEEE Transactions on Circuits and Systems for Video Technology*, 32(12): 8217–8226.
- Jiang, Y.; Gong, X.; Liu, D.; Cheng, Y.; Fang, C.; Shen, X.; Yang, J.; Zhou, P.; and Wang, Z. 2021. Enlightengan: Deep light enhancement without paired supervision. *IEEE transactions on image processing*, 30: 2340–2349.
- Johnson, J.; Alahi, A.; and Fei-Fei, L. 2016. Perceptual losses for real-time style transfer and super-resolution. In *Computer Vision—ECCV 2016: 14th European Conference, Amsterdam, The Netherlands, October 11–14, 2016, Proceedings, Part II 14*, 694–711. Springer.
- Land, E. H.; and McCann, J. J. 1971. Lightness and retinex theory. *Josa*, 61(1): 1–11.
- Li, C.; Guo, C.; Han, L.; Jiang, J.; Cheng, M.-M.; Gu, J.; and Loy, C. C. 2021. Low-light image and video enhancement using deep learning: A survey. *IEEE transactions on pattern analysis and machine intelligence*, 44(12): 9396–9416.
- Liu, R.; Ma, L.; Zhang, J.; Fan, X.; and Luo, Z. 2021. Retinex-inspired unrolling with cooperative prior architecture search for low-light image enhancement. In *Proceedings of the IEEE/CVF conference on computer vision and pattern recognition*, 10561–10570.
- Lore, K. G.; Akintayo, A.; and Sarkar, S. 2017. LLNet: A deep autoencoder approach to natural low-light image enhancement. *Pattern Recognition*, 61: 650–662.
- Ma, L.; Liu, R.; Zhang, J.; Fan, X.; and Luo, Z. 2021. Learning deep context-sensitive decomposition for low-light image enhancement. *IEEE Transactions on Neural Networks and Learning Systems*, 33(10): 5666–5680.
- Ranft, B.; and Stiller, C. 2016. The role of machine vision for intelligent vehicles. *IEEE Transactions on Intelligent vehicles*, 1(1): 8–19.
- Tang, L.; Ma, J.; Zhang, H.; and Guo, X. 2022. DRLIE: Flexible low-light image enhancement via disentangled representations. *IEEE transactions on neural networks and learning systems*, 35(2): 2694–2707.
- Wang, R.; Xu, X.; Fu, C.-W.; Lu, J.; Yu, B.; and Jia, J. 2021. Seeing dynamic scene in the dark: A high-quality video dataset with mechatronic alignment. In *Proceedings of the IEEE/CVF International Conference on Computer Vision*, 9700–9709.
- Wang, T.; Zhang, K.; Shen, T.; Luo, W.; Stenger, B.; and Lu, T. 2023. Ultra-high-definition low-light image enhancement: A benchmark and transformer-based method. In *Proceedings of the AAAI Conference on Artificial Intelligence*, volume 37, 2654–2662.
- Wang, Z.; Bovik, A.; Sheikh, H.; and Simoncelli, E. 2004. Image quality assessment: from error visibility to structural similarity. *IEEE Transactions on Image Processing*, 13(4): 600–612.
- Wang, Z.; Cun, X.; Bao, J.; Zhou, W.; Liu, J.; and Li, H. 2022. Uformer: A general u-shaped transformer for image restoration. In *Proceedings of the IEEE/CVF conference on computer vision and pattern recognition*, 17683–17693.
- Wei, C.; Wang, W.; Yang, W.; and Liu, J. 2018. Deep retinex decomposition for low-light enhancement. *arXiv preprint arXiv:1808.04560*.
- Xu, X.; Wang, R.; Fu, C.-W.; and Jia, J. 2022. Snr-aware low-light image enhancement. In *Proceedings of the IEEE/CVF conference on computer vision and pattern recognition*, 17714–17724.
- Yang, W.; Wang, S.; Fang, Y.; Wang, Y.; and Liu, J. 2021a. Band representation-based semi-supervised low-light image enhancement: Bridging the gap between signal fidelity and perceptual quality. *IEEE Transactions on Image Processing*, 30: 3461–3473.
- Yang, W.; Wang, W.; Huang, H.; Wang, S.; and Liu, J. 2021b. Sparse gradient regularized deep retinex network for robust low-light image enhancement. *IEEE Transactions on Image Processing*, 30: 2072–2086.
- Zamir, S. W.; Arora, A.; Khan, S.; Hayat, M.; Khan, F. S.; and Yang, M.-H. 2022. Restormer: Efficient transformer for high-resolution image restoration. In *Proceedings of the IEEE/CVF conference on computer vision and pattern recognition*, 5728–5739.
- Zamir, S. W.; Arora, A.; Khan, S.; Hayat, M.; Khan, F. S.; Yang, M.-H.; and Shao, L. 2020. Learning enriched features for real image restoration and enhancement. In *Computer Vision—ECCV 2020: 16th European Conference, Glasgow, UK, August 23–28, 2020, Proceedings, Part XXV 16*, 492–511. Springer.
- Zhang, Y.; Zhang, J.; and Guo, X. 2019. Kindling the darkness: A practical low-light image enhancer. In *Proceedings of the 27th ACM international conference on multimedia*, 1632–1640.
- Zhou, S.; Li, C.; and Loy, C. C. 2022. LEDNet: Joint Low-light Enhancement and Deblurring in the Dark. arXiv:2202.03373.

Checklist

- This paper:
 - Includes a conceptual outline and/or pseudocode description of AI methods introduced (yes/partial/no/NA)
 - Yes.
 - Clearly delineates statements that are opinions, hypothesis, and speculation from objective facts and results (yes/no)
 - Yes.
 - Provides well marked pedagogical references for less-familiares readers to gain background necessary to replicate the paper (yes/no)
 - Yes.
- Does this paper make theoretical contributions? (yes/no)
 - Yes.
 - If yes, please complete the list below.
 - All assumptions and restrictions are stated clearly and formally. (yes/partial/no)
 - Yes.

- All novel claims are stated formally (e.g., in theorem statements). (yes/partial/no)
Yes.
- Proofs of all novel claims are included.(yes/partial/no)
Partial.
- Proof sketches or intuitions are given for complex and/or novel results. (yes/partial/no)
Yes.
- Appropriate citations to theoretical tools used are given. (yes/partial/no)
- All theoretical claims are demonstrated empirically to hold. (yes/partial/no/NA)
Yes.
- All experimental code used to eliminate or disprove claims is included. (yes/no/NA)
Yes.
- Does this paper rely on one or more datasets? (yes/no)
Yes
If yes, please complete the list below.
 - A motivation is given for why the experiments are conducted on the selected datasets (yes/partial/no/NA)
Yes.
 - All novel datasets introduced in this paper are included in a data appendix. (yes/partial/no/NA)
Yes.
 - All novel datasets introduced in this paper will be made publicly available upon publication of the paper with a license that allows free usage for research purposes. (yes/partial/no/NA)
Yes.
 - All datasets drawn from the existing literature (potentially including authors' own previously published work) are accompanied by appropriate citations. (yes/no/NA)
Yes.
 - All datasets drawn from the existing literature (potentially including authors' own previously published work) are publicly available. (yes/partial/no/NA)
Yes.
 - All datasets that are not publicly available are described in detail, with explanation why publicly available alternatives are not scientifically satisfying. (yes/partial/no/NA)
Yes
- Does this paper include computational experiments? (yes/no)
Yes
If yes, please complete the list below
 - Any code required for pre-processing data is included in the appendix. (yes/partial/no).
Yes.
 - All source code required for conducting and analyzing the experiments is included in a code appendix. (yes/partial/no)
Yes.
- All source code required for conducting and analyzing the experiments will be made publicly available upon publication of the paper with a license that allows free usage for research purposes. (yes/partial/no)
Yes.
- All source code implementing new methods have comments detailing the implementation, with references to the paper where each step comes from (yes/partial/no)
Partial.
- If an algorithm depends on randomness, then the method used for setting seeds is described in a way sufficient to allow replication of results. (yes/partial/no/NA)
Yes.
- This paper specifies the computing infrastructure used for running experiments (hardware and software), including GPU/CPU models; amount of memory; operating system; names and versions of relevant software libraries and frameworks. (yes/partial/no)
Yes.
- This paper formally describes evaluation metrics used and explains the motivation for choosing these metrics. (yes/partial/no)
Yes.
- This paper states the number of algorithm runs used to compute each reported result. (yes/no)
Yes.
- Analysis of experiments goes beyond single-dimensional summaries of performance (e.g., average; median) to include measures of variation, confidence, or other distributional information. (yes/no)
Yes.
- The significance of any improvement or decrease in performance is judged using appropriate statistical tests (e.g., Wilcoxon signed-rank). (yes/partial/no)
Yes.
- This paper lists all final (hyper-)parameters used for each model/algorithm in the paper's experiments. (yes/partial/no/NA)
Partial. They can be found in the config file of the code that will be published later.
- This paper states the number and range of values tried per (hyper-) parameter during development of the paper, along with the criterion used for selecting the final parameter setting. (yes/partial/no/NA)
Partial.